Final Technical Report for "Regimes of Kinetic Magnetic Reconnection in the Laboratory",

Award Number: DE-SC0019153,

PI: Jan Egedal

UW-Madison award number: MSN219966

Award period: 8/1/18 - 7/31/21

1 Executive summary

The DOE award No. DE-SC0019153, supported in part one graduate student (J. Olson) and material expenses, enabling the student to prepare a basic plasma physics experiment on magnetic reconnection (which we now call the Terrestrial Reconnection Experiment, TREX) within at the Wisconsin Plasma Physics Laboratory (WiPPL). The study of the collisionless magnetic reconnection constituted the primary research carried out under this grant and lead to new observations of unexpected shock formation below the TREX reconnection layer. The shock formation was found fundamental to regulating the normalized rate of reconnection, and the results were part of our experimental observations detailed in a paper first authored by Dr. J. Olson and now published in the Journal of Plasma Physics. In this Report we review the general motivation of this work and provide an overview of our experimental results enabled by the support through the award.

2 TREX and The Problem of Magnetic Reconnection

Magnetic reconnection is the process of breaking magnetic topology and reconstructing it in a less energetic configuration, thereby releasing magnetic energy [1]. Reconnection is a crucial mechanism of particle energization in many different space environments, such as at the solar corona or at the Earth's magnetopause, and evidence for extra-solar reconnection has observed and published [2–4], but despite this ubiquity in space plasma environments, the fundamentals of the process are not well understood. The first theory of reconnection was based on a simple resistive MHD model, but this was later shown to be too slow when compared to observations of actual reconnection events, such as the ejection of solar flares [5–7]. Since then, magnetic reconnection has been broken up into a number of different models that exist across a parameter space characterized by relative system size and Lundquist number. Simulations and observed phenomena cover all areas of this parameter space, but experiments have had more difficulty in breaking out of the reconnection models defined by the lowest system sizes and Lundquist numbers [8].

The divide in this space between the reconnection plasmas that can be approximated as purely hydrodynamic models and the plasmas in which kinetic effects become comparable or even dominant over fluid effects is of particular importance. The most extreme cases of kinetic reconnection are known as "collisionless" reconnection, meaning that the particle collision time is greater than or equal to the time it takes for a particle to transit through the reconnection region. This is the case for reconnection at the Earth's magnetopause [9–11]. This "colli-

sionless" condition facilitates anisotropic velocity distributions that would otherwise be mixed away. Generally, this anisotropy is characterized by the reconnection exhaust be biased toward the direction parallel to the magnetic field. Simulation work demonstrates that these cases also feature distinctive current geometries: namely, the width of the reconnection current layer will be below the ion-scale on comparable to the electron scale and the outflow currents elongate into "jets" that are several times the ion-scale in length [12, 13]. There is as-of-yet no single analytic model that explains why these features develop, but these simulation results have been confirmed by the MMS mission's in-situ measurements at the magnetopause [14–16].

The Terrestrial Reconnection EXperiment is implemented on the Wisconsin Plasma Physics Laboratory (WiPPL), a plasma user facility based at the University of Wisconsin-Madison that operates several plasma experiments that focus on fusion plasmas as well as and space and astrophysical plasmas [17]. The TREX vacuum vessel, provided by WiPPL, is a 3 meter diameter sphere that uses an array of permanent magnets embedded in the chamber wall to limit the plasma loss area to a very narrow fraction of the total surface area. The extent of this cusp magnetic field is far smaller than the vessel's radius; the result is a plasma that is confined over a timescale on the order of multiple milliseconds while simultaneously being unmagnetized through its bulk volume. This allows any number of magnetic field configurations to be implemented inside TREX without disrupting the confinement. These configurations can be created and measured using the large number of available ports of different shapes and sizes along the vessel's outer wall. The TREX setup also includes a permanent exterior Helmholtz coil that is available for use if desired.

TREX's first experimental setup was tested in late 2014, with continued iterations and experimental runs continuing through the present. In 2016, TREX published its first major results- the observation of the formation and ejection of multiple magnetic islands, or "plasmoids," that characterize the multiple X-line collisionless regime of magnetic reconnection [18]. Since then, the focus of TREX has been to probe deeper into the collisionless regime by redesigning and refining the experimental setup to access higher Lundquist numbers and measure the reconnection features at smaller length and time scales.

3 Experimental Configuration

The experimental setup is shown in Fig. 1, outlining the location of the primary TREX components and diagnostics applied in our research so far. The configuration closely resembles that presented in [18], but with a new reconnection drive system consisting of up to four 0.92 m radius reconnection drive coils pulsed by a low-inductance 1 mF capacitor bank. A 10 ms plasma is initiated by an array of pulsed plasma guns [19] with a steady state axial magnetic field from the Helmholtz coil. The drive coils are pulsed with currents in the opposite direction compared to those in the Helmholtz coil. As the currents increase and new magnetic flux is injected by the drive coils, a reconnection current layer forms and is driven toward the central axis. Figure 1b)(8) shows a 2D profile of the resulting toroidal Hall magnetic fields and poloidal field lines to be discussed in more detail below. The stronger drive permits increased voltages at the coils by a factor of 10–100 compared to the earlier TREX experiments. The background plasma temperature and density profiles as functions of R are shown in Fig. 1(c). Similar to reconnection at Earth's dayside magnetopause [20], the plasma density across the reconnection layer includes asymmetries (by about a factor of 3 in this particular discharge).

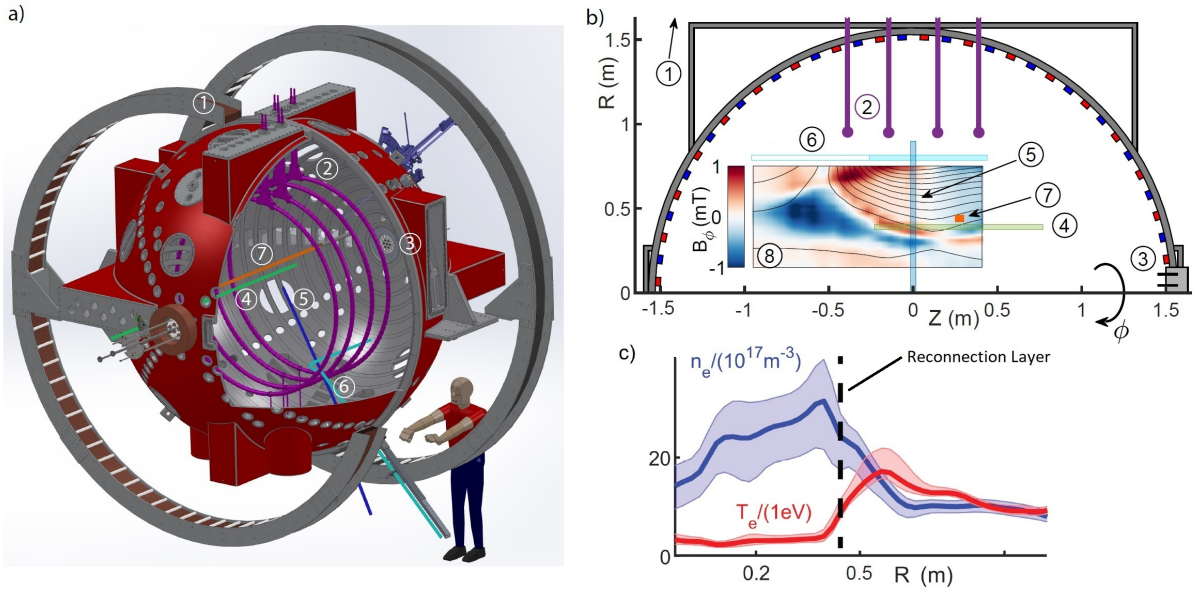

Figure 1: a) A 3D CAD rendering and b) poloidal cross section of the TREX configuration. The primary hardware consists of *(1)* the external Helmholtz coil (at $R = 2$ m), *(2)* the internal reconnection drive coils, and *(3)* the plasma gun array added to the 3 m spherical vacuum vessel. The diagnostics consist of three linear $\dot{B}$ arrays, *(4)* the linear probe, *(5)* the speed probe, and *(6)* the hook probe, as well as *(7)* the T_e probe. The colored segments in b) indicate each probe's spatial coverage. *(8)* An example 2D profile of the toroidal Hall magnetic fields as measured by probe *(6)*. c) Measured profiles of the plasma density n, and electron temperature T_e as functions of radius, in a cut across the reconnection layer (at $R \simeq 0.4$ m).

The experiments utilize a combination of magnetic and electrostatic diagnostics. The colored segments in figure 1(b) show the spatial extent for each probe assembly in the poloidal R–ϕ plane. There are two linear arrays consisting of 14 individual 3-axis $\dot{B}$ probes, the linear probe and the hook probe. The linear probe, spanning 1 m in the Z direction at $R = 0.4$ m, can be scanned to different Z locations. The hook probe enters the device at $Z = -0.25$ m parallel to R before bending 90° to cover 0.8 m in the Z direction at varying R positions. This array can reach from $Z = -0.95$–0.45 m as indicated by the light blue segments in figure 1(b) by rotating 180° around its shaft. Additionally, the speed probe is a stationary array of single-axis $\dot{B}$ probes spanning from $R = 0$–0.9 m at $Z = 0$ m while measuring $\partial B_Z/\partial t$. Finally, located at $R = 0.4$ m and scanned in Z, an electrostatic probe similar to one used in previous TREX work measures the full I-V plasma characteristic by individually biasing 16 closely spaced Langmuir electrodes. This T_e probe and the hook probe are toroidally offset from the linear probe by 18° and 145° respectively.

At large scale, the reconnection dynamics driven in the TREX configuration are highly reproducible for a given configuration. Figure 2 shows example profiles of the reconnection geometry for a discharge in hydrogen gas (H_2) with a drive voltage $V_{\text{drive}} = 5$ kV and Helmholtz field $B_H = 5$ mT. The evolution of the magnetic configuration is characterized by scanning the hook probe to different radial locations over ∼50 discharges with the same experimental settings. At $\Delta t = 0$ µs, the reconnection geometry is already established. As time increases from top to bottom, the reconnection layer of high toroidal current density J_ϕ propagates from $R = 0.55$ m to $R = 0.31$ m with velocity $v_{\text{layer}} \simeq 40$ km/s. This current layer separates the two reconnection inflows with reversed axial magnetic field B_Z shown in figure 2(i-l).

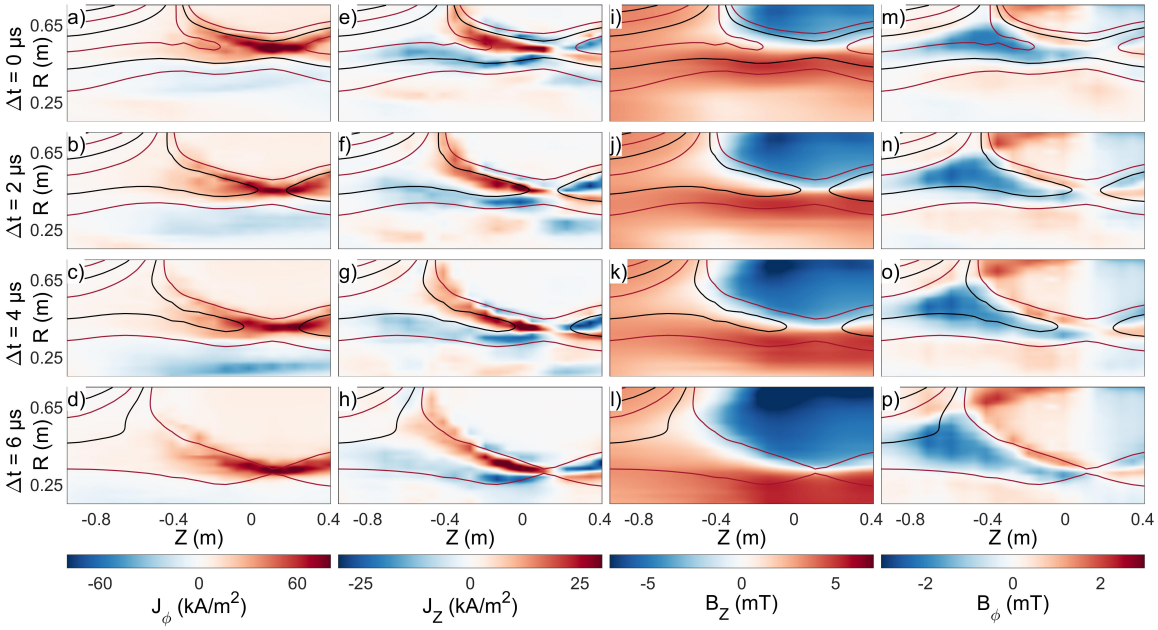

Figure 2: Profiles of (a-d) the toroidal current density J_ϕ, (e-h) the poloidal current density J_Z, (i-l) the reconnecting magnetic field B_Z, and (m-p) the toroidal Hall magnetic field B_ϕ at different times during a shot in H_2 with $B_H = 5$ mT and $V_{\text{drive}} = 5$ kV. The current layer geometry remains roughly constant while propagating from $R = 0.55$ m to $R = 0.31$ m.

The overlaid field lines are contours of constant magnetic flux, coinciding with the poloidal (in-plane) projection of magnetic field lines. All panels consider the same set of contour levels such that the motion of the field lines can be followed in time. Within the two inflow regions, the field lines are all observed to move downward, with those above the reconnection layer moving faster than the layer and those below the layer moving slower than the layer such that in the frame of the reconnection layer, the rate at which field lines are reconnected is roughly constant in time. While the length of the reconnection exhaust does increase slightly in time, the structure of the inner part of the reconnection region is steady as it translates to lower values of R.

4 Shock Front and Magnetic Flux Pileup

The TREX experiment operates in a low collisional regime where Hall physics becomes important [18]. An example event is presented in figure 3 in H_2 with $V_{\text{drive}} = 5$ kV and $B_H = 5$ mT. The data in figure 3(a-c), taken from figure 2 at $\Delta t = 4$ μs, includes the reconnecting magnetic field component B_Z as well as profiles of the toroidal current J_ϕ and in-plane Hall current J_Z. The steady motion of the reconnection layer demonstrated in figure 2 and the nearly constant layer speed shown in figure **??** facilitates the "jogging" method applied to obtain the profiles of electron density n_e, plasma floating potential Φ_f, and electron temperature T_e in figure 3(d-f) measured by the T_e probe at fixed $R = 0.4$ m and varying Z over multiple discharges. The time traces at each Z position are converted to a radial chord of measurements with

$$R' = R - R_0 = (t - t_0) v_{\text{layer}} \,, \tag{1}$$

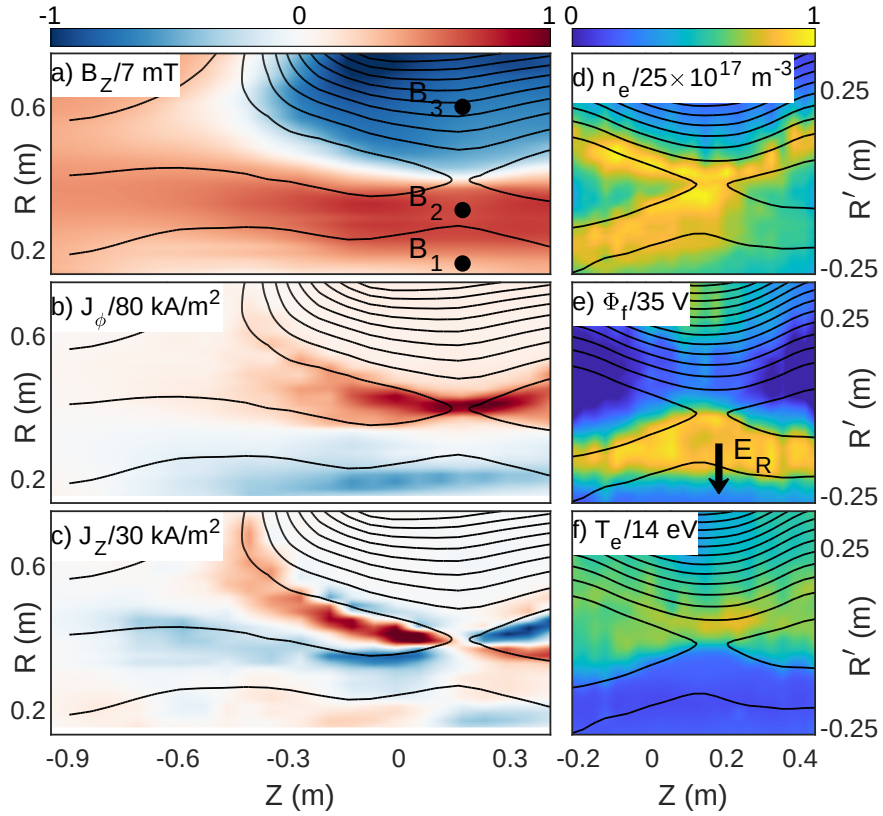

Figure 3: Profiles of a reconnection discharge in H_2 with $B_H = 5$ mT and $V_{\text{drive}} = 5$ kV. (a-c) The reconnecting magnetic field B_Z, toroidal current density J_ϕ, and poloidal current density J_Z are reconstructed from a radial scan with the hook probe array. Contours of constant Ψ are overlaid in black representing the poloidal magnetic field lines. (d-f) The electron density n_e, plasma floating potential Φ_f, and electron temperature T_e measured by scanning the electrostatic probe along Z at $R = 0.4$ m. Here, $R' = t' v_{\text{layer}}$ indicates the radial profile inferred from the temporal probe signal centered around $R = 0.4$ m.

where t_0 is the time the current layer passes $R_0 = 0.4$ m. The density profile is asymmetric with larger densities at low R. In the vicinity of the reconnection region the floating potential in figure 3(e) has a structure similar to that observed by the Cluster mission during reconnection in the Earth's magnetotail [21]. In addition, a sharp jump in the potential structure, $\Delta\Phi_s \simeq 15$ V, is observed at $R' \simeq -0.2$ m providing evidence of a collisionless shock normal electric field E_R.

The far upstream plasma (low R) acts as the leading inflow, and its speed, in the frame of the reconnection layer, typically exceeds the local Alfvén speed. This upstream inflow must therefore be throttled in order for reconnection to take place at the appropriate rate. Thus, a region of magnetic pileup is observed to interface between the reconnection and upstream regions. Figure 4(a) shows a diagram of this configuration in which the upstream region, denoted by the color blue, is separated from the red reconnection layer by a shock in green and a region of pileup in purple. The differences are clear in figure 4(b) where an increase from the upstream field corresponds with a negative spike in toroidal current, driven by the electron $E \times B$-drift with E_R and B_Z. The surface current density across the shock can then be estimated as $K = en_e\Delta\Phi_s/B \simeq 1.6\,\text{kA/m}$, which is in agreement with the observed magnetic pileup of $\Delta B = \mu_0 K \simeq 2$ mT across the shock. The radial electric field E_R is also responsible for reducing the speed of the incoming ions traveling across the shock.

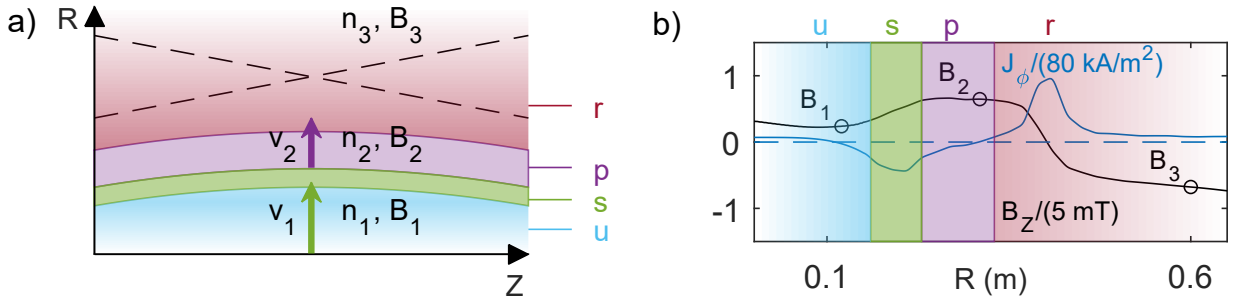

Figure 4: (a) A cartoon depiction of different regions within a TREX discharge. As the current layer is driven into the background plasma, a shock interface (green) separates a region of pileup (purple) from the far upstream (blue), preceding the reconnection layer (red). (b) Radial profiles of B_Z and J_ϕ along a cut through the X-line ($Z = 0.17$ m) in figure 3.

As a consequence of the high Lundquist number regime ($S > 10^3$) in which TREX operates, the negative toroidal current is not expected to be an inductive response to the inward-moving reconnection current sheet. Outside the diffusion region, the pressure tensor and electron inertia terms in Ohm's law can be neglected such that $\mathbf{E} + \mathbf{v_e} \times \mathbf{B} \simeq \eta \mathbf{J}$. Using the experimental parameters within the shock we find $\eta J_\phi \simeq 5 \cdot 10^{-5}\ \Omega\mathrm{m} \times 30\ \mathrm{kA/m^2} = 1.5\ \mathrm{V/m}$, which is much smaller than the typical inductive electric field $|E_\phi| \simeq 50$ V/m. Therefore, in the shock layer, $\mathbf{E} \simeq -\mathbf{v_e} \times \mathbf{B}$ and the role of E_ϕ is to drive radial flows of the electron fluid such that this fluid strictly follows the radial motion of the magnetic field lines.

The profiles in figure 4 provide a qualitative picture of the TREX configurations whereas the exact details, how fast each layer moves or the amount of pileup, depend both on the reconnection dynamics as well as the imposed experimental settings. The gas species, number of plasma guns, Helmholtz field, and drive voltage all control certain aspects of a reconnection event. Figure 5 highlights how the magnetic field evolves throughout a shot for three different cases with varying gas, B_H, and V_{drive}. Each individual probe trace from the speed probe is normalized to 1 mT and offset by its respective radial location, mapping out the magnetic field as the layer moves past each probe toward the central axis. The solid red line indicates the trajectory of the layer where $B_Z = 0$ mT. The red dashed segment marks the region of interest corresponding to $R = 0.4$ m, the radial location of other probes, and where the following analysis is completed. Compared to figure 5(a) with $v_{\mathrm{layer}} = 33$ km/s, the layer in figure 5(b) only moves at 22 km/s, indicative of the heavier ion species. Additionally, both v_{layer} and B_{rec} increase with V_{drive} when comparing figure 5(a,c). In each case, a shock front, indicated by the green line, propagates at a speed $v_{\mathrm{pile}} > v_{\mathrm{layer}}$ ahead of the current layer as it is driven into the relatively stationary bulk plasma. The shock compresses the upstream field to match the allowable reconnection rate, setting how quickly magnetic flux is transferred through the diffusion region, and thereby resulting in the observed B_{rec} and v_{layer}.

Figure 5 presents a subset of the larger overall scan performed on TREX consisting of 882 total shots. All possible combinations of gas (H_2, D, and He) and number of plasma guns (2 and 6 guns) with sets of Helmholtz field (2-7 mT) and drive voltage (1-8 kV) were explored, encompassing 90 different configurations of ~10 shots each. Sets of B_H and V_{drive} were chosen to roughly balance each other in order to create reconnection layers that are only slightly asymmetric. Extreme cases of V_{drive} relative to B_H (or the inverse) are not considered here.

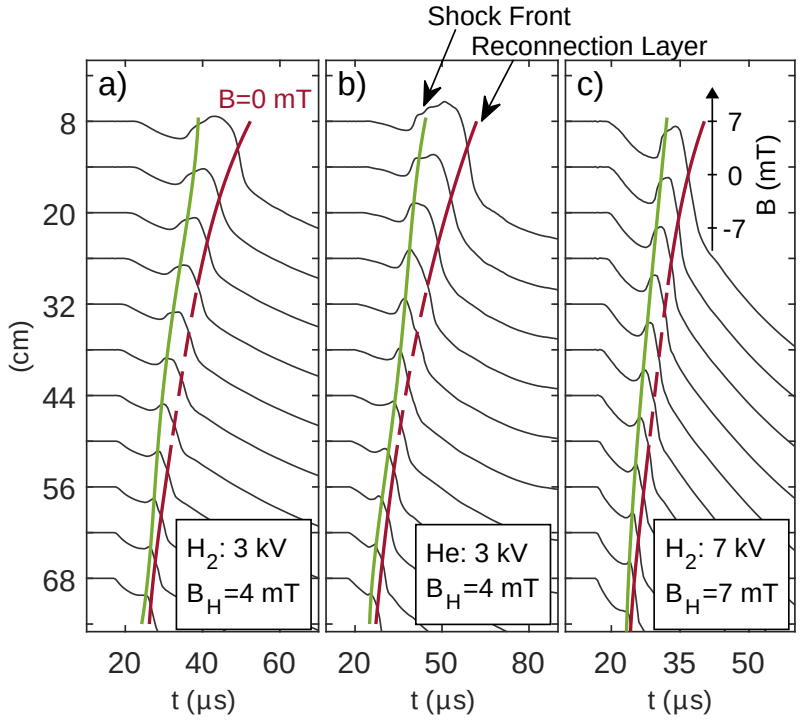

Figure 5: (a-c) Stack plots of magnetic field versus time from the speed probe for three different cases. The scales are normalized such that 1 mT=1 cm and offset by the R location of each probe. The changing time axes are indicative of the difference in timescales for these discharges. The red line follows the $B = 0$ mT contour while the green line indicates the shock front leading the current layer.

In previous flux pileup studies [22, 23], the areas where the magnetic field is increasing are considered a part of the pileup region. Similarly, we consider the observed shock formation as an integral part of the pileup dynamics. While the drive imposes the absolute reconnection rate, it is the pileup magnetic field that largely controls the normalized rate of reconnection such that a stronger pileup magnetic field yields a lower normalized rate. Furthermore, the reconnection rate adheres to an intrinsic scaling that is a function of the normalized system size, L/d_i, and it is this scaling that sets the pileup field magnitude. The shock formation described in the present section is then required to facilitate force balance between the far upstream and pileup regions in a way that is consistent with the Rankine-Hugoniot jump conditions for shocked flows [24–27].

To properly account for the flowing mass into and out of the shock interface, the ram pressure in addition to magnetic and plasma pressure must be included in the total pressure,

$$P_\alpha = m_i n_\alpha v_\alpha^2 + \frac{B_\alpha^2}{2\mu_0} + n_\alpha T_\alpha \,, \tag{2}$$

where the subscript α corresponds to individual regions indicated in the simplified drawing in figure 4(a). Flux and particle continuity provide further constraints on the allowable parameters such that

$$\frac{n_1}{B_1} = \frac{n_2}{B_2} \,, \quad \frac{n_1}{v_2} = \frac{n_2}{v_1} \,, \tag{3}$$

where subscripts 1 and 2 correspond to the upstream and pileup regions, respectively. Using 2

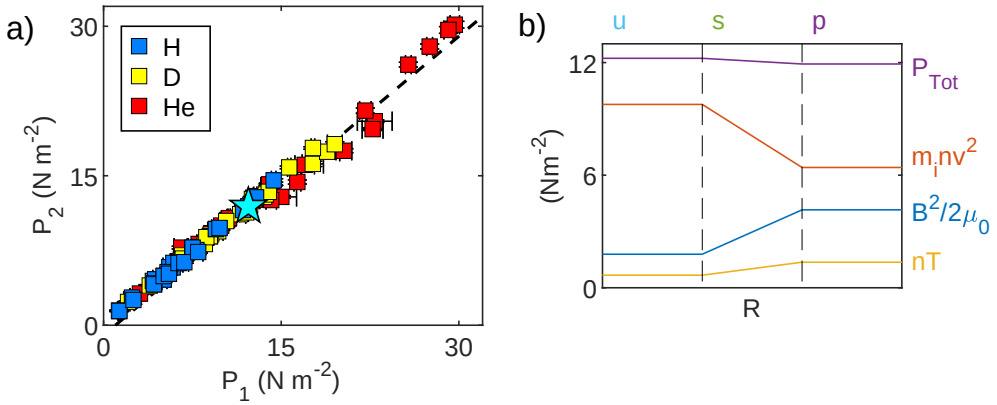

Figure 6: (a) A comparison of the total pressures P_1 and P_2 for all configurations in the dataset. In many cases, the standard deviation error falls below the marker size. (b) Depiction of the change in total pressure along with ram, magnetic, and plasma pressures for the case indicated by the blue star (the event in figure 3) going from the upstream (u) to the pileup (p) regions across the shock interface (s).

and 3, the total pressures for both regions across the shock interface are then

$$P_1 = m_i n_1 v_1^2 + \frac{B_1^2}{2\mu_0} + n_1 T_1 \ , \quad P_2 = m_i n_1 v_1^2 \frac{B_1}{B_2} + \frac{B_2^2}{2\mu_0} + n_1 T_2 \frac{B_2}{B_1} \ , \tag{4}$$

where $T = T_e + T_i \simeq T_e$ throughout the experiment. The velocities in 4 are described in the frame of the shock layer, but v_1 can simply be taken as v_{pile}, the shock velocity measured in the lab frame. Typical values for v_{pile} range from $1.1M_{\text{MS}}$ to $1.5M_{\text{MS}}$, where M_{MS} is the magnetosonic Mach number. As seen in figure 8 of [27], for the observed plasma beta of $\beta \sim 0.1$ on TREX, the critical Mach number at which all ions will be reflected from an incoming perpendicular shock is ~2.7, well above the observed range of v_{pile} for these experiments. Additionally, the electron inertial length $d_e \sim 1$ cm at the shock front is larger than the characteristic magnetic Reynolds length scale, $L_m = \eta/(\mu_0 v_{\text{pile}}) \sim 0.1$ cm. Therefore, the observed shocks tend to steepen to the size of a few d_e wide, consistent with a sub-critical dispersive (rather than resistive) shock [27].

The upstream and pileup pressures are easily computed from measurements and are plotted in figure 6(a) where each data point corresponds to the average of all shots for a single configuration in the parameter scan. The dashed line of slope 1 shows good agreement between the total pressure on either side of the shock front and that force balance is satisfied across the interface regardless of the externally imposed conditions. Pressure profiles for the configuration in figure 3 are given in figure 6(b) which shows a discrete drop in ram pressure across the shock front that is largely balanced by a rise in magnetic pressure such that the total pressure remains nearly constant.

For this set of experiments, shocks are observed to form in all Hydrogen and Deuterium cases and most of the Helium cases. Deriving a strict drive-threshold for the shock formation is difficult with the given dataset as the background magnetic field and drive voltage are not fully independent. Rather, B_H is adjusted within a range that decreases with decreasing reconnection drive. Furthermore, after triggering the reconnection drive but before the reconnection and shock layers have fully formed, the background field declines, which is most pronounced at higher V_{drive}. The upstream Alfvén speed of the shock is then indirectly related to the reconnection drive. In other experiments not presented here, shock formation is not found to occur for $V_{\text{drive}} < 300$ V in Hydrogen.

The TREX configuration is perhaps unusual in the sense that reconnection is only driven from one side of the reconnection layer. Because of the strong magnetic fields associated with the drive, on the side where the drive is applied the Alfvén speed becomes large. Meanwhile, for the undriven side, the Alfvén speed is low and allows for supersonic flows and shock formation not seen in symmetrically driven experiments. While shock fronts on either side of a reconnection layer could easily be envisioned in space and astrophysical situations where supersonic plasma winds collide, such configurations are not easily obtained in laboratory experiments relying on a magnetic drive. It is possible that they can be obtained in laser-driven reconnection experiments, but here the plasma beta is often so large that the magnetic field plays a limited role in setting the overall plasma dynamics [28].

References

[1] E. G. Zweibel and M. Yamada, "Perspectives on magnetic reconnection," *Proc. R. Soc. A Math. Phys. Eng. Sci.*, vol. 472, no. 2196, 2016.

[2] J. Dungey, "Conditions for the occurence of electrical discharges in astrophysical systems," *Philosophical Magazine*, vol. 44, p. 725, 1953.

[3] V. M. Vasyliunas, "Theoretical models of magnetic field line merging," *Reviews of Geophysics*, vol. 13, no. 1, pp. 303–336, 1975.

[4] D. A. Uzdensky, B. Cerutti, and M. C. Begelman, "Reconnection-powered linear accelerator and gamma-ray flares in the crab nebula," *The Astrophysical Journal*, vol. 737, p. L40, Aug 2011.

[5] E. N. Parker, "SWEET'S MECHANISM FOR MERGING MAGNETIC FIELDS IN CONDUCTING FLUIDS," *J. Geophys. Res.*, vol. 62, p. 509, dec 1957.

[6] P. A. Sweet, "The production of high energy particles in solar flares," *Nuovo Cimento Suppl.*, vol. 8, p. 188, Jan 1958.

[7] D. Biskamp, "Magnetic reconnection via current sheets," *The Physics of Fluids*, vol. 29, no. 5, pp. 1520–1531, 1986.

[8] H. Ji and W. Daughton, "Phase diagram for magnetic reconnection in heliophysical, astrophysical, and laboratory plasmas," *Physics of Plasmas*, 2011.

[9] F. Porcelli, D. Borgogno, F. Califano, D. Grasso, M. Ottaviani, and F. Pegoraro, "Recent advances in collisionless magnetic reconnection," *Plasma Physics and Controlled Fusion*, vol. 44, pp. B389–B405, Nov 2002.

[10] L. J. Chen, M. Hesse, S. Wang, D. Gershman, R. E. Ergun, J. Burch, N. Bessho, R. B. Torbert, B. Giles, J. Webster, C. Pollock, J. Dorelli, T. Moore, W. Paterson, B. Lavraud, R. Strangeway, C. Russell, Y. Khotyaintsev, P. A. Lindqvist, and L. Avanov, "Electron diffusion region during magnetopause reconnection with an intermediate guide field: Magnetospheric multiscale observations," *J. Geophys. Res.*, vol. 122, pp. 5235–5246, May 2017.

[11] S. A. Fuselier, S. K. Vines, J. L. Burch, S. M. Petrinec, K. J. Trattner, P. A. Cassak, L. J. Chen, R. E. Ergun, S. Eriksson, B. L. Giles, D. B. Graham, Y. V. Khotyaintsev, B. Lavraud, W. S. Lewis, J. Mukherjee, C. Norgren, T. D. Phan, C. T. Russell, R. J. Strangeway, R. B. Torbert, and J. M. Webster, "Large-scale characteristics of reconnection

diffusion regions and associated magnetopause crossings observed by MMS," *J. Geophys. Res.*, vol. 122, pp. 5466–5486, May 2017.

[12] A. Le, J. Egedal, J. Ng, H. Karimabadi, J. Scudder, V. Roytershteyn, W. Daughton, and Y. H. Liu, "Current sheets and pressure anisotropy in the reconnection exhaust," *Physics of Plasmas*, vol. 21, no. 1, 2014.

[13] A. Le, J. Egedal, W. Daughton, V. Roytershteyn, H. Karimabadi, and C. Forest, "Transition in electron physics of magnetic reconnection in weakly collisional plasma," *Journal of Plasma Physics*, vol. 81, p. 305810108, Jan 2015.

[14] W. Daughton, "Electromagnetic properties of the lower-hybrid drift instability in a thin current sheet Electromagnetic properties of the lower-hybrid drift instability in a thin current sheet," *Phys. Plasmas*, vol. 3103, no. 2003, 2017.

[15] J. Egedal, A. Le, W. Daughton, B. Wetherton, P. A. Cassak, L. J. Chen, B. Lavraud, R. B. Torbert, J. Dorelli, D. J. Gershman, and L. A. Avanov, "Spacecraft Observations and Analytic Theory of Crescent-Shaped Electron Distributions in Asymmetric Magnetic Reconnection," *Physical Review Letters*, 2016.

[16] A. Le, J. Egedal, O. Ohia, W. Daughton, H. Karimabadi, and V. S. Lukin, "Regimes of the electron diffusion region in magnetic reconnection," *Physical Review Letters*, 2013.

[17] C. B. Forest, K. Flanagan, M. Brookhart, M. Clark, C. M. Cooper, V. Desangles, J. Egedal, D. Endrizzi, I. V. Khalzov, H. Li, M. Miesch, J. Milhone, M. Nornberg, J. Olson, E. Peterson, F. Roesler, A. Schekochihin, O. Schmitz, R. Siller, A. Spitkovsky, A. Stemo, J. Wallace, D. Weisberg, and E. Zweibel, "The Wisconsin Plasma Astrophysics Laboratory," *J. Plasma Phys.*, vol. 81, pp. 1–22, oct 2015.

[18] J. Olson, J. Egedal, S. Greess, R. Myers, M. Clark, D. Endrizzi, K. Flanagan, J. Milhone, E. Peterson, J. Wallace, D. Weisberg, and C. B. Forest, "Experimental Demonstration of the Collisionless Plasmoid Instability below the Ion Kinetic Scale during Magnetic Reconnection," *Phys. Rev. Lett.*, vol. 116, no. 25, pp. 1–5, 2016.

[19] G. Fiksel, A. F. Almagri, D. Craig, M. Iida, S. C. Prager, and J. S. Sarff, "High current plasma electron emitter," *Plasma Sources Science & Technology*, vol. 5, pp. 78–83, FEB 1996.

[20] J. L. Burch, T. E. Moore, R. B. Torbert, and B. L. Giles, "Magnetospheric Multiscale Overview and Science Objectives," *Space Science Reviews*, vol. 199, pp. 5–21, MAR 2016.

[21] J. R. Wygant, C. A. Cattell, R. Lysak, Y. Song, J. Dombeck, J. McFadden, F. S. Mozer, C. W. Carlson, G. Parks, E. A. Lucek, A. Balogh, M. Andre, H. Reme, M. Hesse, and C. Mouikis, "Cluster observations of an intense normal component of the electric field at a thin reconnecting current sheet in the tail and its role in the shock-like acceleration of the ion fluid into the separatrix region," *J. Geophys. Res. Sp. Phys.*, vol. 110, pp. 1–30, sep 2005.

[22] M. Øieroset, T. D. Phan, J. F. Drake, J. P. Eastwood, S. A. Fuselier, R. J. Strangeway, C. Haggerty, M. A. Shay, M. Oka, S. Wang, L. J. Chen, I. Kacem, B. Lavraud, V. Angelopoulos, J. L. Burch, R. B. Torbert, R. E. Ergun, Y. Khotyaintsev, P. A. Lindqvist, D. J. Gershman, B. L. Giles, C. Pollock, T. E. Moore, C. T. Russell, Y. Saito, L. A. Avanov, and W. Paterson, "Reconnection With Magnetic Flux Pileup at the Interface of Converging Jets at the Magnetopause," *Geophys. Res. Lett.*, vol. 46, no. 4, pp. 1937–1946, 2019.

[23] J. C. Dorelli and J. Birn, "Whistler-mediated magnetic reconnection in large systems: Magnetic flux pileup and the formation of thin current sheets," *J. Geophys. Res. Sp. Phys.*, vol. 108, no. A3, 2003.

[24] W. J. Macquorn Rankine, "On the Thermodynamic Theory of Waves of Finite Longitudinal Disturbance," tech. rep., 1870.

[25] P. H. Hugoniot, "Mémoire sur la propagation du mouvement dans les corps et ples spécialement dans les gaz parfaits, 1e Partie," *Paris J. Ec. Polytech*, vol. 57, p. 3, 1887.

[26] P. H. Hugoniot, "Mémoire sur la propagation du mouvement dans les corps et plus spécialement dans les gaz parfaits, 2e Partie," *Paris J. Ec. Polytech*, vol. 58, p. 1, 1889.

[27] C. F. Kennel, J. P. Edmiston, and T. Hada, "A Quarter Century of Collisionless Shock Research," in *Collisionless Shock. Heliosph. A Tutor. Rev. Vol. 34*, vol. 34, ch. 1, pp. 1–36, mar 1985.

[28] W. Fox, A. Bhattacharjee, and K. Germaschewski, "Fast magnetic reconnection in laser-produced plasma bubbles," *Phys. Rev. Lett.*, vol. 106, no. 21, pp. 1–4, 2011.